Biophysical Chemistry 159 (2011) 237–246

Contents lists available at ScienceDirect

Biophysical Chemistry

journal homepage: http://www.elsevier.com/locate/biophyschem

A few low-frequency normal modes predominantly contribute to conformational responses of hen egg white lysozyme in the tetragonal crystal to variations of molecular packing controlled by environmental humidity

Yuki Takayama, Masayoshi Nakasako *

Department of Physics, Faculty of Science and Technology, Keio University, 3-14-1 Hiyoshi, Kohoku-ku, Kanagawa 223-8522, Japan
The RIKEN Harima Institute/SPring-8, 1-1-1 Kouto, Mikaduki, Sayo, Hyogo, 679-5148, Japan

ARTICLE INFO

Article history:
Received 30 May 2011
Received in revised form 3 July 2011
Accepted 3 July 2011
Available online 13 July 2011

Keywords:
Conformational change
Humidity control
Normal mode analysis
Protein dynamics
X-ray crystallography

ABSTRACT

The structures of proteins in crystals are fixed by molecular interactions with neighboring molecules, except in non-contacting flexible regions. Thus, it is difficult to imagine what conformational changes occur in solution. However, if molecular interactions can be changed by manipulating molecular packing in crystals, it may be possible to visualize conformational responses of proteins at atomic resolution by diffraction experiments. For this purpose, it is suitable to control the molecular packing in protein crystals by changing the volume of solvent channels through variation of the environmental relative humidity. Here, we studied conformational responses of hen egg white lysozyme (HEWL) in the tetragonal crystal by X-ray diffraction experiments using a humidity-control apparatus, which provided air flow of 20–98%rh at 298 K. First, we monitored the lattice parameters and crystalline order during dehydration and rehydration of HEWL crystal between 61 and 94%rh at 300 K. Then two crystal structures at a resolution of 2.1 Å using diffraction data obtained at 84.2 and 71.9%rh were determined to discuss the conformational responses of HEWL against the external perturbation induced by changes in molecular packing. The structure at 71.9%rh displayed a closure movement that was likely induced by the molecular contacts formed during dehydration and could be approximated by ten low-frequency normal modes for the crystal structure obtained at 84.2%rh. In addition, we observed reorganization of hydration structures at the molecular interfaces between symmetry neighbors. These findings suggest that humidity-controlled X-ray crystallography is an effective tool to investigate the responses of inherent intramolecular motions of proteins to external perturbations.

1. Introduction

X-ray crystallography has contributed to reveal conformational variations in proteins arising from plasticity and dynamics [1]. For instance, conformational differences between the various crystal forms of a protein can be used to identify flexible regions and understand how protein molecules respond to external perturbations [2]. In addition, the meta-stable states in protein domain movements trapped during crystallization provide information regarding the energy landscape of proteins, including hydration structures [3]. However, such crystallographic observations are still pieces of luck and rarely encountered in protein crystal structure analyses. To allow experimental visualization of possible conformational variations at atomic resolution, the systematic control of intramolecular motions of proteins is necessary.

Fig. 1 illustrates a proposed scheme to control conformations of protein molecules in a crystal, in which solvent channels occupy more than 30% of the volume [4]. When a protein crystal is exposed to dry conditions, water molecules of solvent channels escape through vapor diffusion at the crystal surface. The loss of these molecules probably induces lattice shrinkage that accompanies the rearrangements and conformational changes of protein molecules. In contrast, the swelling of solvent channels under wet conditions results in weak intermolecular contacts. Thus, the control of molecular packing modes by adjusting the relative humidity (RH) around protein crystals is likely applicable for the study of conformational responses of proteins against external perturbations [2].

In early crystallographic studies aimed at controlling the RH surrounding protein crystals, various simple techniques were attempted using salt solutions of known RH [2,5–10] and oil [11]. Recently, several apparatus that use RH-controlled air flow have been developed to finely adjust the RH around protein crystals [12–14].

Abbreviations: ASA, accessible surface area; ERH, equilibrium relative humidity; H-bond, hydrogen bond; HEWL, hen egg white lysozyme; RH, relative humidity; r.m.s., root-mean-square; TLS, translation-libration-screw.

* Corresponding author. Department of Physics, Faculty of Science and Technology, Keio University, 3-14-1 Hiyoshi, Kohoku-ku, Kanagawa 223-8522, Japan. Tel.: +81 45 566 1679; fax: +81 45 566 1672.
E-mail address: nakasako@phys.keio.ac.jp (M. Nakasako).

0301-4622/$ – see front matter © 2011 Elsevier B.V. All rights reserved.
doi:10.1016/j.bpc.2011.07.001

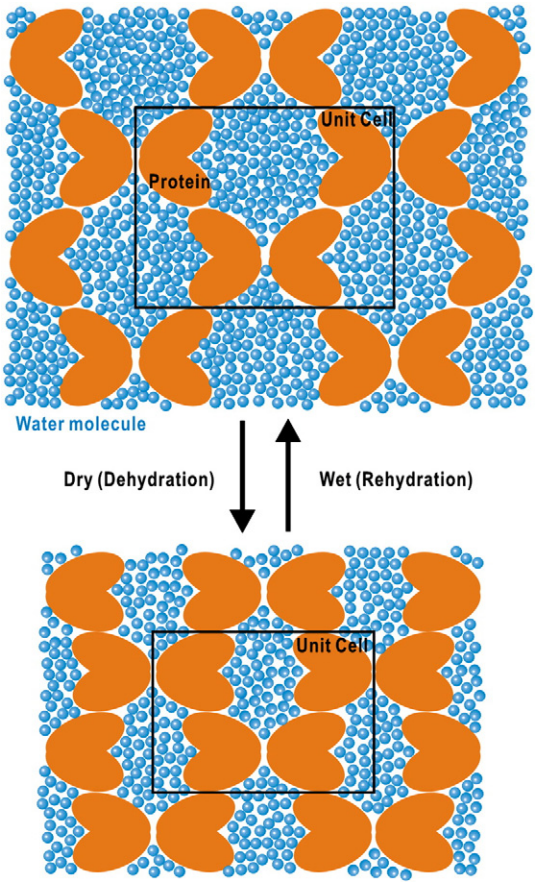

Fig. 1. A schematic illustration to explain the influences of RH changes around protein crystals on the molecular packing mode, protein conformations and solvent content.

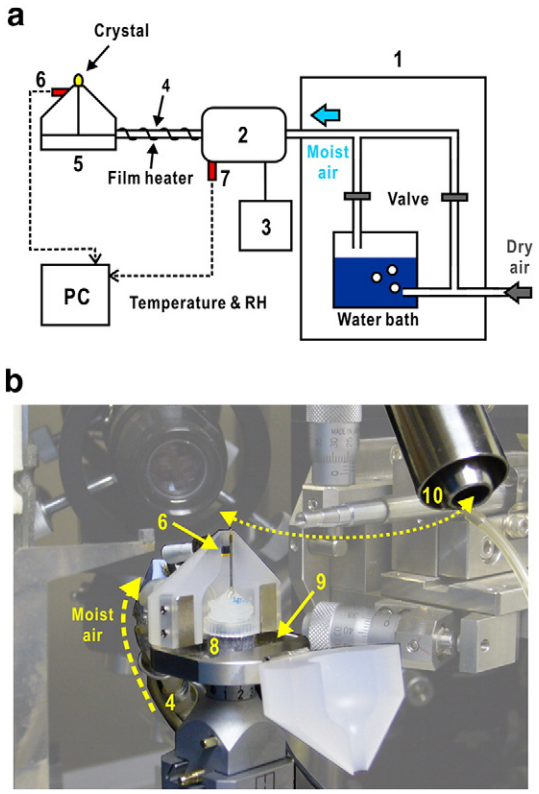

Fig. 2. (a) A schematic diagram of our custom-made RH-control apparatus, which was composed of a HUM-1 moist air generator (1), humidity-controlling chamber (2), thermal circulator (3), transfer tube warmed with a film heater (4), crystal holder (5), and sensors simultaneously measuring the temperature and RH (6 and 7). (b) A photograph showing the crystal holder attached on a goniometer head. The crystal holder equipped with a neodymium magnet (8) fixes a crystal mounting device (Crystal Cap; Hampton Research). The platform of the holder (9) has a guide for a cryo-tong to remove the mounting device after flash-cooling. Humidity-controlled crystals were quickly flash-cooled by rotating the exit nozzle for a low-temperature nitrogen gas flow (10).

Those apparatus have been utilized to improve molecular arrangements in protein crystals for high resolution structure analyses [12,14–18]. However, the potential of these latest RH-control techniques to finely control protein conformations in crystals has not yet been demonstrated.

To explore the feasibility of RH control in the investigation of conformational responses of proteins to external perturbations, here, we conducted X-ray diffraction experiments for tetragonal crystals of hen egg white lysozyme (HEWL) using a custom-made RH-control apparatus. Accompanying the RH-dependent shrinkage of solvent channels and the alternation in the molecular packing mode, HEWL displayed a global conformational change that resulted in a closure of the active-site cleft. This observation allowed us to discuss a mechanism for the RH-dependent responses of the unit cell and the relevance of the RH-induced conformational changes to the inherent intramolecular motions of HEWL.

2. Materials and methods

2.1. Apparatus for RH-controlled X-ray diffraction experiment

Our custom-made apparatus for RH-controlled X-ray diffraction experiment was mainly composed of a HUM-1 moist air generator (Rigaku, Japan) and a crystal holder (Fig. 2). The generator produced RH-controlled air flow of 300–450 ml/min by mixing dry and moisture-saturated air. The mixing ratio was automatically tuned to produce air flow with a desired RH by monitoring the RH inside a RH-controlling chamber attached to the generator. The temperature inside the RH-controlling chamber was kept constant using a thermal circulator (TAITEC, Japan) to suppress fluctuations in RH. A flexible transfer tube, which connected the chamber and the crystal holder, was warmed by a film heater to prevent dew formation. When the temperatures of the RH-controlling chamber and transfer tube were set at 303 and 308 K, respectively, the apparatus provided RH-controlled air flow of up to 98%rh at the sample position in the crystal holder with a fluctuation of 2%rh at 298 K ± 0.4 K.

The crystal holder attached to a goniometer head (Huber, Germany) was composed of a platform with a neodymium magnet and a pair of PCTFE (Daiflon) blocks on hinges (Fig. 2b). The pair of blocks had a chamber for a Crystal Cap mounting device (Hampton Research, USA). Crystals were mounted on a MicroMesh film of 400/10 or 400/25 type (MiTeGen LLC, USA) glued to the crystal mounting device. When the mounting device was placed in the chamber, crystals were positioned approximately 2 mm above the upper edge of the blocks. The pair of blocks was fabricated into a cone shape to record diffraction patterns up to a resolution of 1.5 Å when using Cu $k\alpha$ radiation. The crystal mounting device could be quickly set by opening one of the hinged blocks. The flexible transfer tube allowed the goniometer to be rotated 180° for the collection of diffraction data under RH-controlled conditions. The hinged blocks of the crystal holder facilitated the quick flash-cooling of RH-controlled protein crystals using a low-temperature nitrogen gas stream.

The temperature and RH around mounted protein crystals were recorded by a SHT75 sensor (Sensirion AG, Switzerland) located 5 mm below the crystal position. The shape and dimensions of crystals were monitored by a CCD camera (Toshiba Teli Co., Japan) connected to a microscope (Thales Optem Inc., USA).

2.2. Preparation of HEWL crystal and determination of its initial equilibrium RH

HEWL (Wako, Japan) was crystallized into the tetragonal form by the hanging-drop vapor diffusion method at 293 K using a precipitant solution containing 3–8% (w/v) NaCl and 100 mM Na acetate (pH 4.2) [19]. For the diffraction experiments, crystals were first dialyzed for 3 h against a buffer containing 25% (w/v) glycerol, 14.6% (w/v) NaCl, and 100 mM Na acetate (pH 4.2) because of the reason described in the Results section.

In RH-controlled X-ray diffraction experiments, protein crystals must be mounted under equilibrium relative humidity (ERH) conditions to avoid degradation caused by changes in environmental RH [12]. Under ERH conditions, the evaporation and adsorption of water on the surfaces of protein crystals were in valance, because the vapor pressure on the protein crystal surfaces was thought to be almost the same with that of the crystal mother liquor. The ERH condition of HEWL crystals was determined by monitoring the droplet size of the mother liquor set in the sample position of the crystal holder with gradual variation of RH. Under ERH conditions, little volume change of the droplet was observed.

2.3. Lattice parameters and quality of HEWL crystal under various RH

To search two RH conditions suitable for crystal structure analysis with different molecular packing, we first measured the RH-dependent variations of the lattice parameters and diffraction patterns of a dialyzed HEWL crystal with a size of $300\times250\times250\ \mu m^3$. The crystal was set under 94%rh at 300 K, and the mother liquor remaining around the crystal was removed using a paper wick for complete exposure of the crystal surfaces to the RH-controlled air flow. The crystal was first dehydrated by decreasing RH at a rate of 4.7%rh/h. After the RH reached 61%rh, a rehydration process was started at a rate of 3.9%rh/h to raise the RH to 92%rh.

The diffraction patterns of HEWL crystals were successively taken every 15 min during the RH variation by the oscillation method using Cu $k\alpha$ radiation ($\lambda = 1.5418$ Å) generated from an Ultrax-18 X-ray generator (Rigaku) operated at 45 kV and 90 mA, a Pt-coated double-focusing mirror system (Rigaku) and an R-axis IV imaging plate detector (Rigaku). The crystal-to-detector distance was 150 mm and the oscillation range was 1.0°/11-min exposure for almost the same orientation of the crystal against the incident X-ray beam. The lattice parameters were determined for each diffraction pattern using the *HKL2000* suite [20].

2.4. Crystal structure analyses under different RH conditions

A dialyzed crystal ($400\times200\times200\ \mu m^3$) was mounted under an RH condition of 84.2%rh at 299.5 K and solvent remaining around the crystal was removed. The *c*-axis of the crystal was inclined slightly from the rotation axis of the goniometer, and the *a*-axis was initially aligned along the incident X-ray beam.

Diffraction data were collected as a series of 1.0° oscillations per 5 min exposure at a sample-to-detector distance of 100 mm using the X-ray diffraction equipment described above. The first set was collected under 84.2 ± 1.1%rh at 300.0 ± 0.5 K. The RH around the crystal was then decreased at a rate of 4.1%rh/h, and the second set was collected under 71.9 ± 0.7%rh at 300.6 ± 0.1 K. To reduce radiation damage, each diffraction data set was limited to cover the minimum volume in reciprocal space necessary for the structural analysis. The indexing, integration, scaling and post-refinement of diffraction data were carried out using the *HKL2000* suite [20].

Structural refinements were performed using the program *REFMAC5*[21] in the *CCP4* suite [22], and the structural models were built using the *COOT* suite [23]. For the refinement against the first data set, we used the crystal structure of HEWL (the accession code in the Protein Data Bank [24]; 1JIS [25]) after removing the solvent molecules as the initial model. For the refinement against the second data set, the crystal structure for the first data set was used. Hydration water molecules and ions were picked up from the electron density peaks that appeared in both the $2F_o–F_c$ and $F_o–F_c$ maps contoured at the 1.0 σ and 2.0 σ levels, respectively. The stereochemistry of the final models was validated by the program *PROCHECK*[26], and the coordinate errors [27] were estimated using the program *SFCHECK* [28]. In addition, we evaluated the contribution of the translation-libration-screw (TLS) motions of HEWL molecules to the B-factors using *REFMAC5* and the *TLSMD* web server [29].

The refined models were compared after being superimposed using the program *LSQKAB*[30]. For evaluating the intermolecular interactions between crystallographic neighbors, we picked up polar (oxygen and nitrogen) atom pairs separated by 2.4–3.4 Å as hydrogen bonds (H-bonds) and other pairs within a distance range of 3.4–3.7 Å as van der Waals contacts. Solvent accessible surface area (ASA) engaged in crystal contacts was calculated using the program *AREAIMOL*[22] with a probe of 1.4-Å radius. Solvent channels were visualized using the *^3V* web server with inner and outer probe radii of 3 Å and 10 Å, respectively [31].

2.5. Normal mode analysis

Normal mode analysis was applied to the crystal structure under 84.2%rh assuming the elastic network model [32,33]. In the model, the structure was approximated as an assembly of 129 Cα atoms and springs connecting atom pairs within a given cut-off distance. The k-th normal mode ($\boldsymbol{\sigma}_k$) contributed to the positional displacement of the i-th Cα atom ($\mathbf{r}_i$) through the eigen matrix (A_{ik}) as $\mathbf{r}_i = \sum_k A_{ik}\boldsymbol{\sigma}_k$. The computation was performed using the *ELASTN* program suite coded by M.N. The trial calculations suggested that a cut-off distance of 9 Å was suitable to maximize the correlation between B-factors from the normal mode analysis and the crystal structure. The force constant was then adjusted to equalize the sum of theoretical and experimental B-factors. In addition, to evaluate the possible contribution of each normal mode to the displacement of the i-th Cα atom ($\Delta\mathbf{r}_i$) between the two crystal structures under the different RH conditions, we calculated the weight (W_k) for the k-th normal mode using the following equation $\Delta\mathbf{r}_i = \sum_k W_k A_{ik}\boldsymbol{\sigma}_k$.

3. Results

3.1. RH-dependent variations of lattice parameters and diffraction patterns

The ERH of the crystallization buffer was 97–98%rh. This was nearly the upper limit of the RH of the moist air flow produced by the RH-control apparatus. Regarding the dialysis buffer, the ERH of 88–89%rh was in the controllable range. The dialyzed HEWL crystals showed little change in the structure and molecular packing mode from those in the crystallization buffer, as described in Section 3.2.

The course of the RH-dependent variations of the dialyzed HEWL crystal was divided into eight stages (I–VIII, Fig. 3). In the RH range of 94–83%rh (stage I), the crystal diffracted X-rays beyond a resolution of 2 Å. When decreasing the RH from 83 to 76%rh (stage II), the unit cell displayed anisotropic shrinkage along the *a*-axis, rather than the *c*-axis. In stage III of 76–65%rh, despite few appreciable changes in the unit cell dimensions, the diffraction patterns gradually degraded to a resolution of 8 Å along with broadening of the diffraction spots. At the beginning of stage IV (65–61%rh), the unit cell suddenly collapsed along the *c*-axis by approximately 3 Å, as reported in an earlier work [5]. Regarding the macroscopic dimensions of the crystal

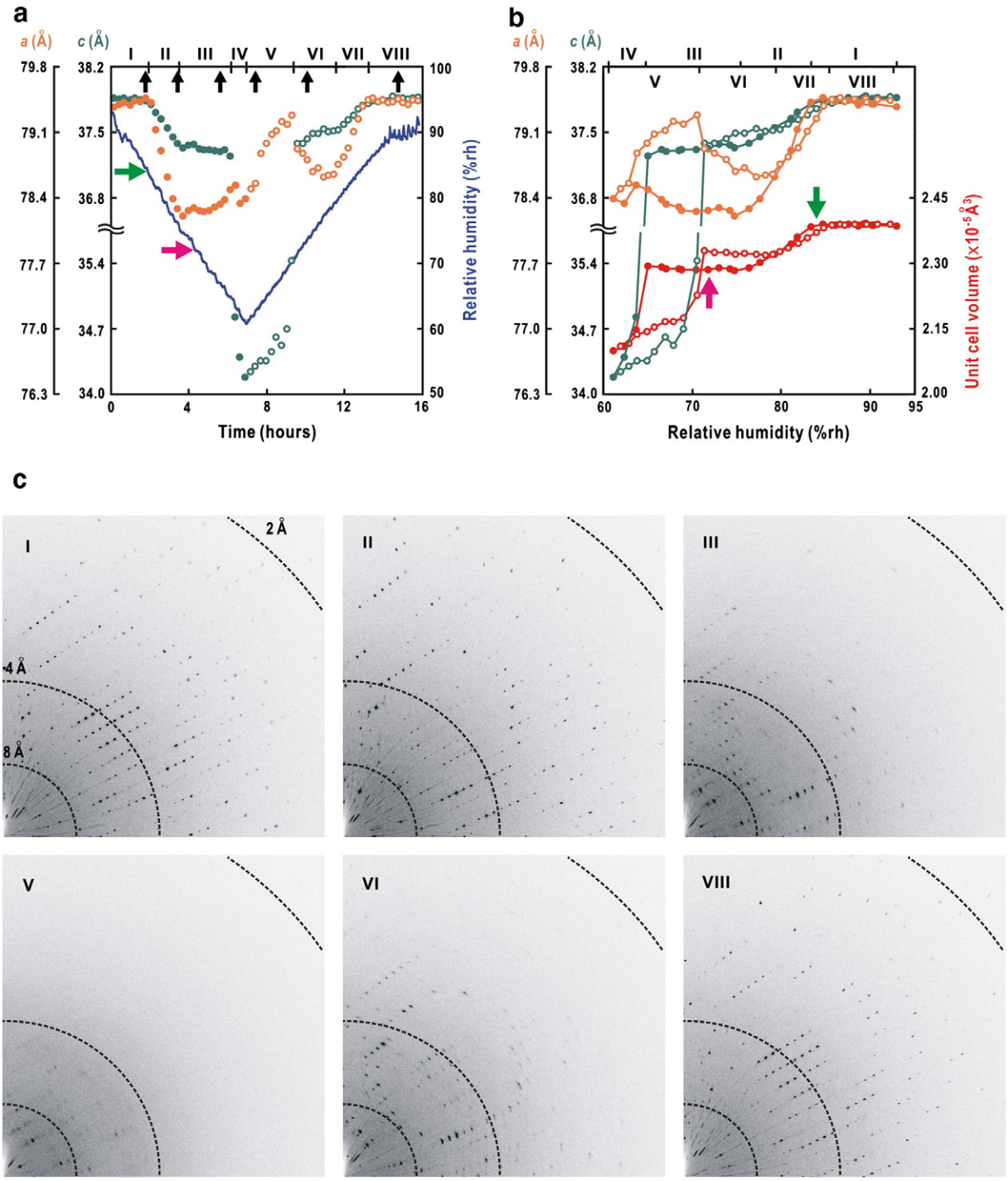

Fig. 3. (a) Time course of the changes in the lattice constants *a* (orange) and *c* (deep green) during changes in the RH (blue line). The filled and open symbols indicate the values in the dehydration and rehydration processes, respectively. Stages I–VIII, which are described in the text, are indicated at the top of the plot. The green and magenta arrows indicate the RH conditions for diffraction data collection of the H- and L-states, respectively. The black arrows indicate when the diffraction patterns in panel (c) were taken in the dehydration/rehydration processes. (b) RH-dependent variations in the lattice constants *a* (orange) and *c* (deep green), and the unit cell volume (red) are plotted against the RH values. The filled and open symbols are used as in panel (a). (c) Diffraction patterns in a quarter of the detector. The patterns were taken at the time indicated by the arrows in panel (a). The stages in the RH variation are labeled in the upper left of each panel.

monitored by the CCD camera, the shrinkage began at stage II and continued to the end of stage IV.

In stage V (61–71%rh), the RH was increased for the rehydration of the crystal. While the crystal quality was little improved, as observed from the diffraction patterns, the volume of the unit cell slightly increased. At 71%rh, the unit cell suddenly expanded along the *c*-axis. In stage VI of 71–79%rh, the resolution limit of the diffraction patterns improved up to 2 Å along with the sharpness of the diffraction spots. As the shrinkage and expansion of the *a*- and *c*-axes, respectively, occurred simultaneously, the unit cell volume was maintained almost constant. The unit cell swelled again in the *a*–*b* plane in stage VII of 79–85%rh. Finally, in stage VIII of 85–92%rh, the lattice parameters

and diffraction patterns recovered to those observed under the initial RH condition. During the rehydration process, the macroscopic expansion of the crystal size was prominent in stages V–VII.

3.2. RH-dependent changes in molecular arrangement

Based on the results described above, we collected diffraction data from one HEWL crystal under two different RH conditions (Fig. 3a–b and Table 1). The first data set was collected under RH of 84.2 ± 1.1%rh (H-state) just prior to stage II, while the second data set was obtained under the RH condition of 71.9 ± 0.7%rh (L-state). The L-state was the lower limit to collect diffraction data at high resolution in stage III, since diffraction patterns degraded rapidly below 72%rh. The crystal structures in the H- and L-states were refined at a resolution of 2.1 Å (Table 1). The structure of HEWL in the H-state displayed a root-mean-square (r.m.s.) difference for main chain atoms of less than 0.3 Å from the initial model used in the refinement, and the arrangement of molecules in the unit cell was almost the same with that in the crystal of the initial model. The structure of the L-state displayed a r.m.s. difference for main chain atoms of 0.6 Å from that of a low-humidity (88%rh) state previously reported from an earlier study (PDB: 4LYM [6]).

The reduction of the solvent content of the unit cell from the H- to the L-state (Table 1) corresponded to the escape of approximately 350 water molecules from three solvent channels (α, β, and γ) running almost parallel to the *c*-axis (Fig. 4a). In addition, the L-state showed an approximately 10-Å^2 higher average B-factor than that of the H-state (Table 1). This increase was likely the result of TLS motions of whole HEWL molecules in their collective positional shifts during the lattice shrinkage rather than from intramolecular motions.

A HEWL molecule in the L-state shifted along the *a*–*b* plane by 1.3 Å with a rotation of 1.6° from those in the H-state, resulting in a narrowed solvent channel α (Fig. 4a). The magnitude of both the shift and the rotation was nearly twice those observed in the earlier work [6]. The number of van der Waals contacts and H-bonds between symmetry-related neighbors increased as a result of the positional shifts, whereas the number of H-bonds mediated by hydration water molecules decreased (Table 2). Following the changes in the number of the contacts, the surface area engaged in direct intermolecular contacts increased by 2% of the total ASA. In addition, the positional shifts of side chains larger than 0.5 Å in Arg14, Asn46, Thr47, Asn59, Gly71, and Arg128 (Fig. 4c) were likely caused by molecular packing in the L-state (Fig. 4b). The most drastic conformational change was found in Asn46, in which the side chain shifted to flip the Asn59 side chain (Fig. 4d).

3.3. Domain closure movement

The local changes in HEWL structure described above were in correlation with a global conformational change that served to close the active-site cleft situated between the small and large lobes (Fig. 5). Each lobe displayed an r.m.s. difference of main chain atoms of less than 0.7 Å between the L- and H-states, while that of all main chain atoms was only 0.2 Å. This finding suggested that the movement of both lobes resulted in closure of the active-site cleft. A similar closure movement, although to a lesser extent, was previously observed at 88%rh [6]. Referring the various types of intramolecular movements of proteins [34], the closure movement was classified as a hinge-bending motion and was probably induced by intermolecular contacts of the lobes with adjacent molecules.

To understand the relevance of the closure movement to the inherent intramolecular motions in HEWL, we compared the directions and magnitudes of the positional shifts of Cα atoms with the displacement vectors expected from the weighted sum of ten low-frequency normal modes of the HEWL molecule in the H-state (Fig. 5a). The sum of the ten low-frequency modes with r.m.s. displacements of larger than 0.02 Å for Cα atoms could approximate the conformational changes from the H- to the L-state. Between the observed and theoretically predicted displacement vectors, the correlation coefficients were 0.94 in magnitude and 0.79 in the direction when taking the magnitudes of positional shifts of the Cα atoms into consideration. In particular, the lowest-energy normal mode (Fig. 5b) dominated the observed conformational changes, as

Table 1
Statistics of the diffraction intensity data and the refined structural models.

	H-state	L-state
RH (%rh) / temperature (K)	84.2 ± 1.1 / 300.0 ± 0.5	71.9 ± 0.7 / 300.6 ± 0.1
Diffraction intensity data		
Space group	$P4_32_12$	$P4_32_12$
Lattice constants *a*, *c* (Å)	79.5, 37.9	78.2, 37.3
Solvent content [a] (%)	41.2	38.4
Resolution (last shell) [b] (Å)	50.0–2.10 (2.18–2.10)	50.0–2.10 (2.18–2.10)
Unique / observed reflections	7214 / 24,569	6466 / 16,899
Completeness [c] (last shell) [b] (%)	95.9 (96.6)	90.1 (86.7)
$<I/\sigma>$ (last shell) [b]	12.5 (10.5)	20.8 (3.3)
R^I_{merge} [d] (last shell) [b]	0.048 (0.085)	0.046 (0.254)
Structure refinement		
Resolution (last shell) [b] (Å)	19.06–2.10 (2.15–2.10)	16.92–2.10 (2.16–2.10)
Number of reflections used	6866	6146
R [e] (last shell) [b] / R_{free} [f] (last shell) [b]	0.155 (0.151) / 0.220 (0.249)	0.160 (0.180) / 0.218 (0.248)
Number of non-H protein atoms	1001	1001
water molecules [g] / acetate / Na / Cl ions	59 / 1 / 2 / 1	54 / 1 / 2 / 1
r.m.s. deviation from ideal bond length (Å) / angle (°)	0.016 / 1.477	0.017 / 1.585
Ramachandran regions (%) Most favored / additionally allowed	90.3 / 9.7	88.5 / 11.5
Coordinate error estimated (Å)	0.19	0.20
Average B factors protein atoms / water molecules (Å^2)	19.8 / 28.8	29.4 / 37.6
PDB accession code	3AW6	3AW7

[a] Solvent contents [50] were calculated using the molecular weight of HEWL (14.3 kDa).
[b] The figures in the parentheses were calculated for the last shell.
[c] The ratio of the numbers of experimental and theoretically expected unique reflections.
[d] $R_{merge}{}^I = \sum_h \sum_i |I_i(h) - <I(h)>| / \sum_h \sum_i I_i(h)$, where $I_i(h)$ is the intensity of *i*-th observation of reflection *h*.
[e] $R = \sum_h |F_{obs}(h) - F_{calc}(h)| / \sum_h F_{obs}(h)$, where $F_{obs}(h)$ and $F_{calc}(h)$ are the observed and calculated structure factors of reflection *h*, respectively.
[f] The R_{free} factor was calculated for 5% of unique reflections, which were not used in the structure refinement throughout [51].
[g] The electron density maps were appreciable for water molecules with B-factors of less than 45 Å^2 in the H-state. In contrast, the maps were inappreciable for molecules with B-factors higher than 60 Å^2 in the L-state, probably because the average B-factor of the L-state was approximately 10 Å^2 higher than that of the H-state.

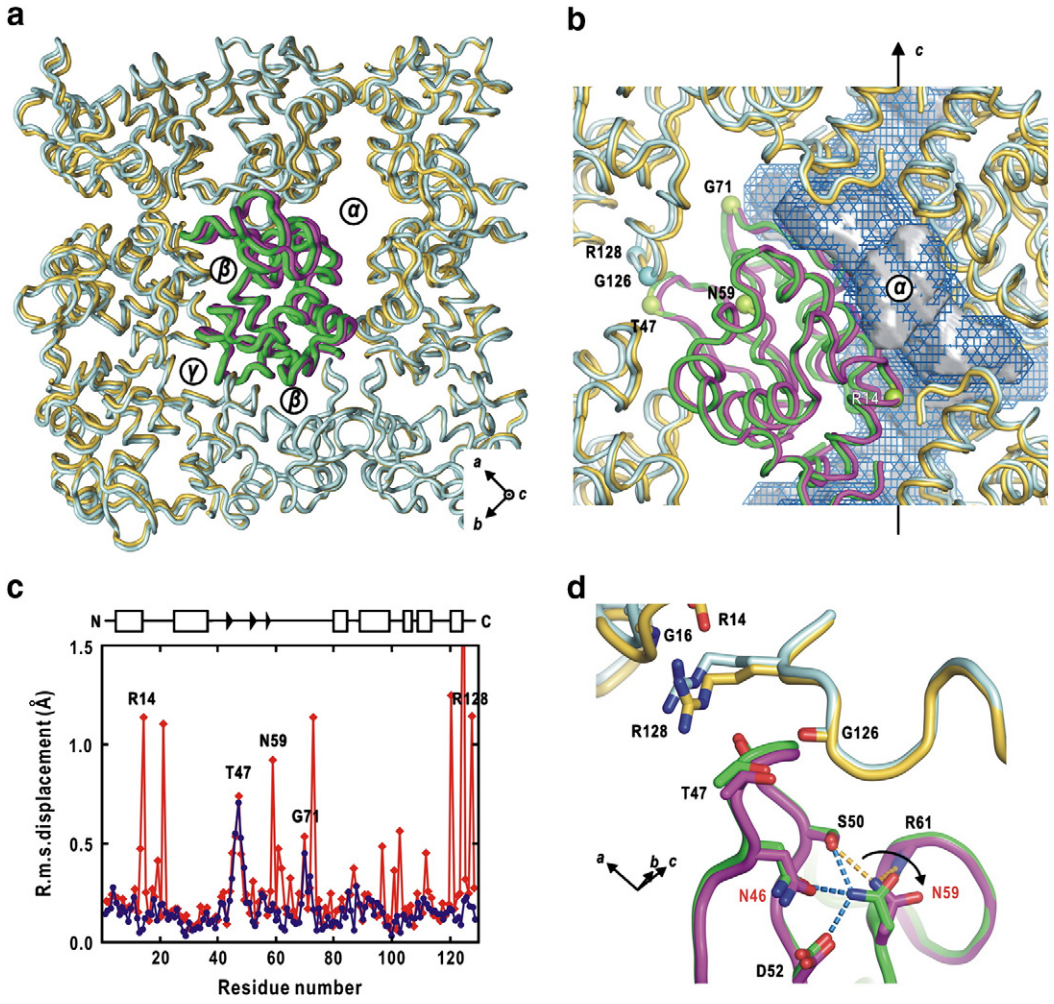

Fig. 4. (a) Comparison of the arrangements of HEWL molecules in H-state (green- or cyan-colored models) and L-state (pink or yellow) crystals. HEWL molecules are drawn as Cα traces. Three solvent channels running along the *c*-axis are labeled as α, β, and γ. (b) Magnified view demonstrating the shrinkage of solvent channel α. The HEWL models are illustrated as in panel (a). The shape of the channel in the H-state (blue mesh) and that in the L-state (gray surface) are compared. The side chains of labeled residues, except Gly126, displayed positional shifts larger than 0.5 Å between the H- and L-states. (c) R.m.s. displacements of main chain (blue) and side chain (red) atoms between the H- and L-states. A diagram of the secondary structure is also shown, with boxes for α-helices and arrows for β-strands. (d) View showing the local conformational changes around residues Thr47 and Asn59 induced by close contact in the L-state. The side chains of residues picked up are shown as atom-colored stick models. The Cα trace models are colored as in panel (b). The dashed cyan and orange lines are possible hydrogen bonds formed by Asn59 in the H- and in L-states, respectively. Panels (a, b, d) were prepared using *PyMOL* [52].

indicated by the correlation coefficients of 0.89 and 0.64 for the positional shifts and direction, respectively. These findings suggested that the energetically most flexible motion in the H-state was excited by the close molecular contacts at both lobes induced by the changes in RH.

Table 2
Number of molecular contacts identified in the H- and L-states.

Number of interactions	H-state	L-state
Between neighboring molecules arranged along the a–b plane		
van der Waals contacts between protein atoms	73	88
H-bonds between protein atoms	29	32
H-bonds mediated by water molecules		
One water molecule	27	23 (23)[a]
Two water molecules	19	12 (11)[a]
Between neighboring molecules arranged along the c-axis		
van der Waals contacts between protein atoms	4	18
H-bonds between protein atoms	2	5
H-bonds mediated by water molecules		
One water molecule	5	3 (3)[a]
Two water molecules	2	2 (2)[a]

[a] The figures in parentheses are the number of molecular contacts mediated by hydration water molecules occupying the hydration site within 1.5 Å from those found in the H-state.

3.4. Hydration structure changes

The RH-dependent shrinkage of the unit cell induced not only positional and conformational changes of HEWL molecules, but also the reorganization of their hydration structures (Fig. 6 and Table 2). In the crystallographic asymmetric unit, we found that 36 water molecules, including 13 engaged in intermolecular contacts, resided in almost the same hydration sites between the H- and L-states (Fig. 6a). The water molecules displayed good correlations in the directions of their displacements with those of the H-bond partner atoms of HEWL molecules (Fig. 6a).

At surface grooves and molecular interfaces of the L-state, we additionally identified 12 hydration water molecules located near hydration sites in the H-state (Fig. 6a). The additional water molecules, which were likely squeezed out from the hydration sites in the H-state by conformational changes of HEWL molecules (Fig. 5), displayed only small directional correlation with their H-bond partners of HEWL (Fig. 6a). In addition, the hydration structure changes caused the loss of several hydration-mediated crystal contacts (Table 2).

Although we identified eight water molecules located at the intermolecular interface and three that were exposed to channel α in the H-state (Fig. 6b), the molecules were inappreciable in the electron

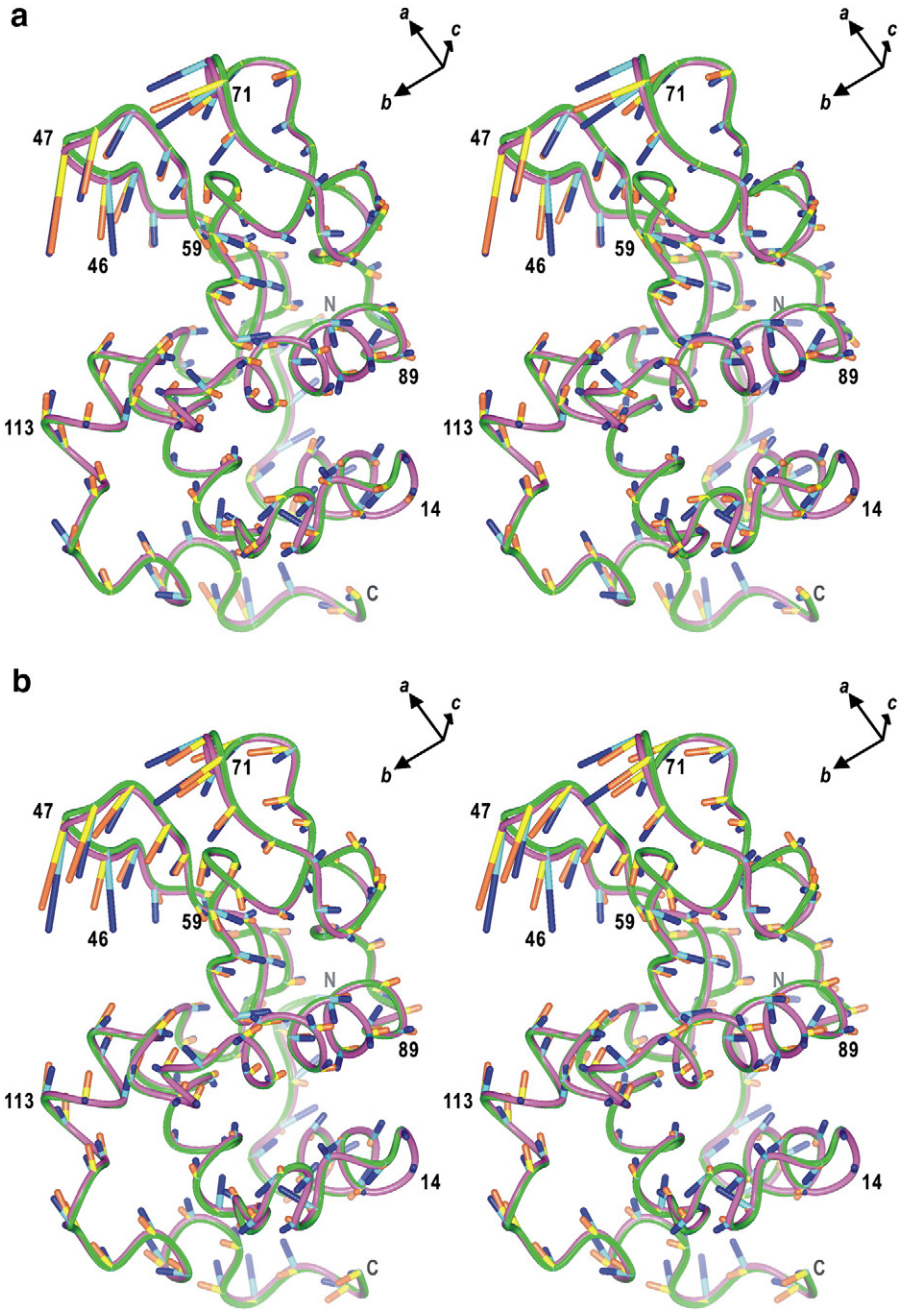

Fig. 5. (a) A stereo view illustrating the global conformational changes between the H-state (green-colored Cα trace model) and the L-state (pink). The models are superimposed with all atoms optimally overlapping. The displacement vectors of Cα atoms are shown by the sticks from the cyan (H-state) to the blue ends (L-state). The sticks from the yellow to the orange ends are displacement vectors calculated from the ten low-frequency normal modes in the H-state. Both vectors are magnified 10 fold for clarity. Several residues, including Asn46 and Asn59, are labeled. (b) A stereo view demonstrating the contribution of the lowest-energy normal mode to the global conformational changes between the H-state (green-colored Cα trace model) and the L-state (pink). The structures, positional shifts and contribution of the normal mode are illustrated as in panel (a). Panels were prepared using *CCP4mg* [53].

density map of the L-state. However, six water molecules were identified only in the L-state at the molecular interface, which was formed in the dehydration process (Fig. 6b).

4. Discussion

In this study, we measured RH-dependent variations of the lattice parameters in a tetragonal HEWL crystal and identified conformational changes induced between 84.2%rh and 71.9%rh. Here, we discuss the molecular mechanisms underlying the observed RH-dependent phenomena in HEWL crystals and the possibility of investigating the inherent protein motions by RH-controlled X-ray crystallography.

4.1. Conformational changes in HEWL

Through theoretical and simulation studies, experimentally visualized structural changes of proteins under external perturbations are proposed to be explained using the linear responses of inherent low-energy dynamics of proteins free from external perturbations [35]. Particularly, a

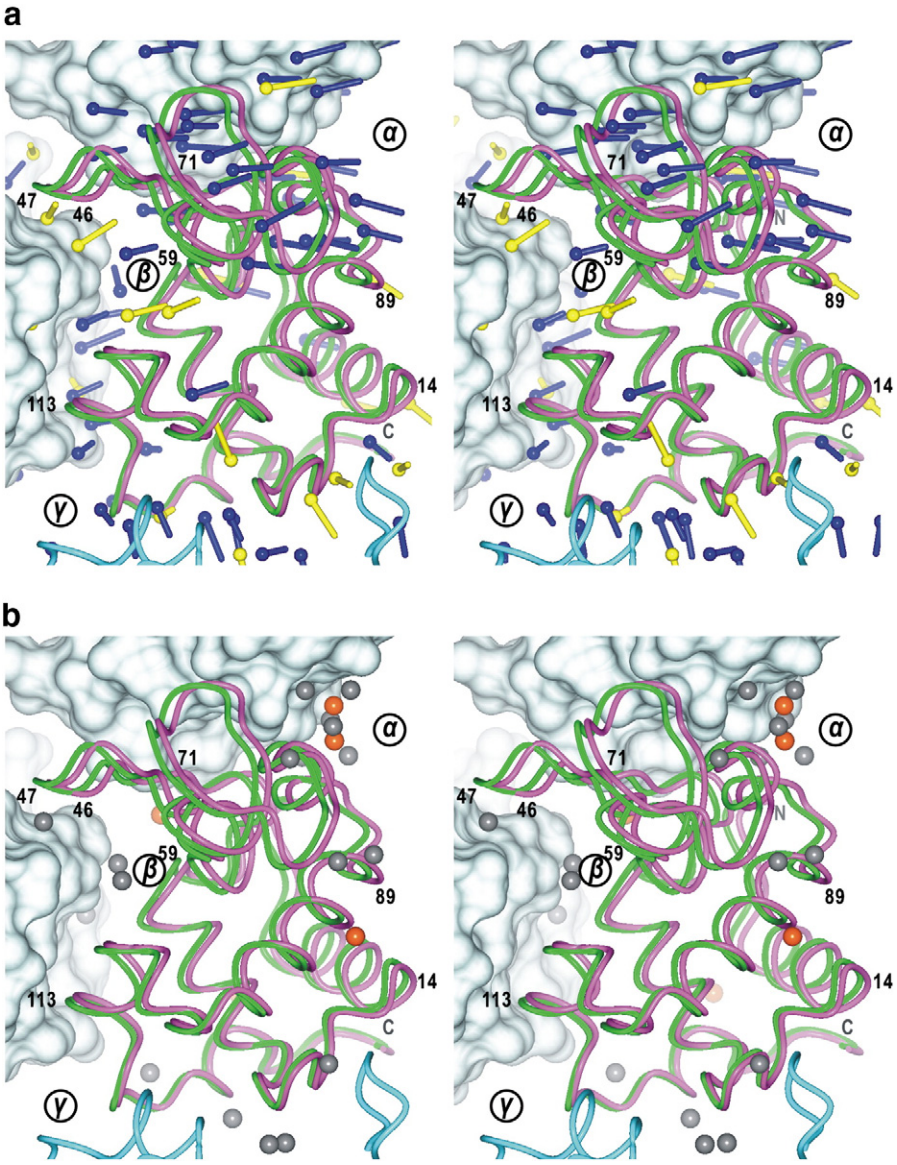

Fig. 6. (a) A stereo plot illustrating the positional shifts of hydration water molecules from the H- to the L-state. The positions of hydration water molecules in the H-state are indicated by balls, and the displacement of the water molecules from the H- to the L-states are illustrated as sticks with 10-fold magnification for clarity. The direction in the displacement of the water molecules in blue coincided with those of their H-bond partners in proteins within 20°, while those of the molecules in yellow were larger than 20°. The HEWL molecules in the H- and L-states are drawn as in Fig. 5, and the cyan-colored surface models and tube models are symmetry-related neighbors. (b) A stereo plot showing the positions of hydration water molecules identified only in the H-state (gray sphere) and only in the L-state (orange).

set of several low-frequency normal modes represents global collective motions in proteins [36]. In addition, the conformational changes in several proteins found between different crystal forms are approximated by low-frequency normal modes [37,38]. The most easily realized conformational changes arise from large equilibrium fluctuations that intrinsically exist in a small number of collective low-frequency normal modes [35].

Based on the theoretical studies of protein dynamics, the observed changes in the molecular packing mode induced by dehydration of the HEWL crystal (Fig. 4a–b) represent external perturbations of molecules, and the conformational changes probably reflect the inherent intramolecular motions of HEWL, as suggested from the normal mode analysis (Fig. 5). Thus, the RH-control technique for protein crystals may serve as an experimental tool to study intrinsic protein motions in the crystalline state by controlling molecular packing modes, as discussed in Section 4.4.

4.2. Influences of changes in molecular packing on hydration structures

In the L-state, approximately 25% of the hydration-mediated molecular contacts observed in the H-state were not found (Table 2), probably due to the exclusion of seven hydration water molecules (Fig. 6). As these water molecules functioned as cushions at the interface between adjacent molecules, their exclusion was necessary for the close packing of HEWL molecules to adapt to the shrinkage of the solvent channels. On the other hand, the presence of confined hydration water molecules at molecular interfaces supposed to facilitate robust intermolecular interactions [39] by tetrahedral H-bond arms [40] to introduce varieties in molecular contacts and by making molecular interfaces complementary [41]. Thus, the exclusion of water molecules probably causes a slight disorder in the molecular arrangements in the L-state, as suggested by the increase in B-factors (Table 1), because the fine tuning of such arrangements is difficult by only direct protein–protein contacts.

Although the present structural analyses were limited to two RH conditions, further fine slice of the RH conditions would allow visualization of the reorganization of hydration structures at the interfaces. Because the exclusion of water molecules confined in a narrow space is similar to the escape of hydration water molecules during the domain motion of an enzyme [42], snapshots of hydration structural changes at molecular interfaces may help to understand the dynamics of hydration structures on protein surfaces. For the purpose, the combinational use of the conventional cryo-technique and the RH-control (Fig. 2) is more effective, as the amount of water molecules trapped on protein surfaces at cryogenic temperature is several times larger than that at ambient temperature [43].

4.3. RH-dependent variations in solvent channels and molecular packing

In the present experiments, the custom-made RH-control apparatus (Fig. 2) and solvent condition that were used to lower the ERH allowed the fine measurement of the RH-dependent anisotropic behavior of cell dimensions and the hysteresis in the dehydration and rehydration cycles (Fig. 3b). Based on the measurement results and the crystal structures of HEWL in the H- and L-states, here, we speculate on the mechanism underlying the RH-dependent variation of the molecular packing mode.

In the dehydration process, water supplied from the solvent channels escapes from the crystal surfaces. Channel α, which has the largest volume and cross-sectional size (Fig. 4a), is thought to be the predominant source of water. This speculation is supported by the greater water permeability along the *c*-axis than that of the *a*–*b* plane [44]. Thus, the observed volume changes of channel α probably drive the shrinkage of the unit cell, particularly along the *a*–*b* plane.

The lattice shrinkage along the *a*–*b* plane in stages I–II is likely relevant to the conformational changes of HEWL molecules between the H- and L-states approximated by the low-frequency normal modes (Fig. 5). Since the two lobes of HEWL molecules lie in the *a*–*b* plane of the tetragonal crystal (Fig. 4a), the positional shifts of HEWL molecules are compensated by the easily excitable closure movement (Fig. 5). However, as there are no wide solvent channels extending along the *a*–*b* plane (Fig. 4b), and HEWL molecules lack low-frequency modes along the short molecular axis, namely along the *c*-axis in the crystal (Fig. 4b), shrinkage in the *c*-axis is probably smaller than that along the *a*–*b* plane (Fig. 3a–b). Further shrinkage of the *c*-axis in stage III induces disorder in the arrangement of molecules, rather than the collective positional shifts observed in stages I–II (Fig. 3b–c). The disordered molecular arrangement may be one of the causes for the closer packing along the *c*-axis observed at the beginning of stage IV (Fig. 3a–b). The interactions caused by the close packing in stage IV are difficult to relax during the rehydration process, and the expansion within the *a*–*b* plane first proceeds to compensate for the expansion of the solvent channels (Fig. 3a–b). Although this represents a speculated mechanism of the observed hysteresis, it is likely relevant to the theoretically predicted mechanical properties of HEWL crystals: plastic along the *a*–*b* plane, but elastoplastic along the *c*-axis [45]. In addition, differences in the molecular contacts between the dehydration and rehydration processes are probably reflected in the reported differences in the sound velocity in HEWL crystals measured by the Brillouin scattering technique [46].

4.4. X-ray diffraction measurements over a wide range of RH to study inherent motions of proteins

RH-dependent conformational changes have been observed for several protein crystals [8,10,14,47]. To date, larger conformational changes, as monitored by the r.m.s. displacement of main chain atoms, are reported to occur under lower RH environments (Fig. 7), although the magnitude of the changes depends on the molecular packing and molecule size. Conformational changes in several regions and domains of such crystal structures are significant because their magnitudes are larger than the coordinate errors in the analyses. It is necessary to examine whether the conformational changes are described by low-frequency normal modes, as demonstrated for HEWL molecule in the present study. However, the reported changes encourage us to investigate the mechanical responses of proteins in the crystalline state by RH-controlled X-ray crystallography. In the next stage of our research, we will attempt to control domain movement in glutamate dehydrogenase to evaluate whether RH-controlled X-ray crystallography is applicable to manipulate large conformational changes.

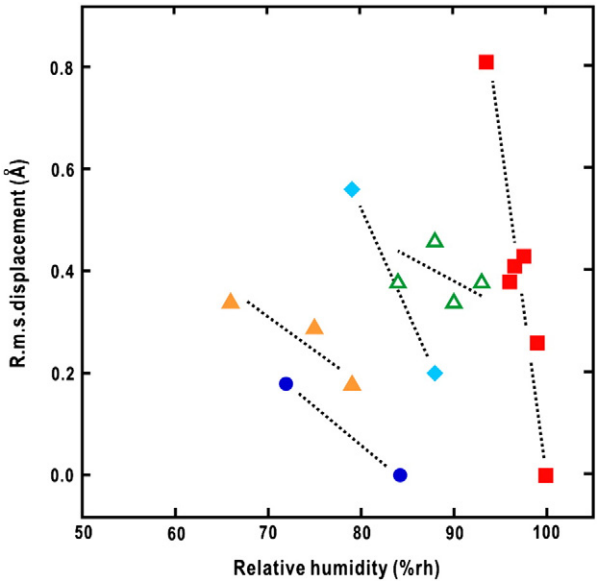

Fig. 7. Plot showing the RH-dependent r.m.s. displacements of main chain atoms under low RH conditions from those of the crystal mother liquors for HEWL (circles; present study), ribonuclease A [8] (diamonds), methaemoglobin [47] (filled triangles), oxyhaemoglobin [10] (open triangles), and F_1-ATPase [14] (squares). The dotted lines indicate tendencies of the RH-dependent changes.

From the experiences in this study, we identified two critical points for the success of RH-controlled X-ray diffraction experiments in the RH range of 61–94%rh (Fig. 3a–b). The first is the low flow rate of our apparatus to allow a quasi-static control of the RH surrounding protein crystals. The evaporation rate from, for instance, a flat surface in a moist laminar air flow is experimentally known to be proportional to the root of the flow rate assuming Fick's diffusion law [48]. Thus, our apparatus would be advantageous for quasi-static and mild evaporation of water at crystal surfaces.

The second important consideration is the reduction in the ERH of HEWL crystals due to the dialysis buffer. This reduction allows the molecular packing in crystals to be controlled in a wider range of RH than the crystallization buffer, the ERH of which is similar to those reported for various crystals (approximately 95%rh) [12,14,17,18]. The ERH reduction in dialysis buffer is probably caused by the presence of glycerol, as expected from its effect on the vapor pressure of aqueous solutions [49]. The presence of glycerol in the crystallization buffer is also advantageous for the flash-cooling of crystals at an optimum RH condition without the necessity for sealing by mineral oil, when a cryo-nozzle is situated near the crystal position, as is found in our apparatus (Fig. 2b).

Acknowledgements

This study was supported by Grants-in-Aid from MEXT (Nos. 15076210, 20050030, 22244054, and 23120525) and JSPS Japan (1920402 and 22018027) to M.N.

References

[1] G.E. Schulz, Domain motions in proteins, Curr. Opin. Struct. Biol. 1 (1991) 883–888.
[2] L. Vijayalakshmi, R. Krishna, R. Sankaranarayanan, M. Vijayan, An asymmetric dimer of β-lactoglobulin in a low humidity crystal form—structural changes that accompany partial dehydration and protein action, Proteins Struct. Funct. Bioinfo. 71 (2008) 241–249.
[3] M. Nakasako, Water–protein interactions from high-resolution protein crystallography, Phil. Trans. R. Soc. Lond. B359 (2004) 1191–1206.
[4] K.A. Kantardjieff, B. Rupp, Matthews coefficient probabilities: improved estimates for unit cell contents of proteins, DNA, and protein–nucleic acid complex crystals, Protein Sci. 12 (2003) 1865–1871.
[5] I. Dobrianov, S. Kriminski, C.L. Caylor, S.G. Lemay, C. Kimmer, A. Kisselev, K.D. Finkelstein, R.E. Thorne, Dynamic response of tetragonal lysozyme crystals to changes in relative humidity: implications for post-growth crystal treatments, Acta Cryst. D57 (2001) 61–68.
[6] R. Kodandapani, C.G. Suresh, M. Vijayan, Crystal structure of low humidity tetragonal lysozyme at 2.1-Å resolution. Variability in hydration shell and its structural consequences, J. Biol. Chem. 265 (1990) 16126–16131.
[7] G.S. Kachalova, V.N. Morozov, T.Ya. Morozova, E.T. Myachin, A.A. Vagin, B.V. Strokopytov, Yu.V. Nekrasov, Comparison of structures of dry and wet hen egg-white lysozyme molecule at 1.8 Å resolution, FEBS Lett. 284 (1991) 91–94.
[8] K.V.R. Kishan, N.R. Chandra, C. Sudarsanakumar, K. Suguna, M. Vijayan, Water-dependent domain motion and flexibility in ribonuclease A and the invariant features in its hydration shell. An X-ray study of two low-humidity crystal forms of the enzyme, Acta Cryst. D51 (1995) 703–710.
[9] H.G. Nagendra, C. Sudarsanakumar, M. Vijayan, An X-ray analysis of native monoclinic lysozyme. A case study on the reliability of refined protein structures and a comparison with the low-humidity form in relation to mobility and enzyme action, Acta Cryst. D52 (1996) 1067–1074.
[10] B.K. Biswal, M. Vijayan, Structures of human oxy- and deoxyhaemoglobin at different levels of humidity: variability in the T state, Acta Cryst. D58 (2002) 1155–1161.
[11] L.M. Hunsicker-Wang, R.L. Pacoma, Y. Chen, J.A. Fee, C.D. Stout, A novel cryoprotection scheme for enhancing the diffraction of crystals of recombinant cytochrome ba_3 oxidase from *Thermus thermophilus*, Acta Cryst. D61 (2005) 340–343.
[12] R. Kiefersauer, M.E. Than, H. Dobbek, L. Gremer, M. Melero, S. Strobl, J.M. Dias, T. Soulimane, R. Huber, A novel free-mounting system for protein crystals: transformation and improvement of diffraction power by accurately controlled humidity changes, J. Appl. Cryst. 33 (2000) 1223–1230.
[13] T. Sjögren, G. Carlsson, G. Larsson, A. Hajdu, C. Andersson, H. Pettersson, J. Hajdu, Protein crystallography in a vapour stream: data collection, reaction initiation and intermediate trapping in naked hydrated protein crystals, J. Appl. Cryst. 35 (2002) 113–116.
[14] J. Sanchez-Weatherby, M.W. Bowler, J. Huet, A. Gobbo, F. Felisaz, B. Lavault, R. Moya, J. Kadlec, R.B.G. Ravelli, F. Cipriani, Improving diffraction by humidity control: a novel device compatible with X-ray beamlines, Acta Cryst. D65 (2009) 1237–1246.
[15] H. Dobbek, L. Gremer, R. Kiefersauer, R. Huber, O. Meyer, Catalysis at a dinuclear [CuSMo(= O)OH] cluster in a CO dehydrogenase resolved at 1.1-Å resolution, Proc. Natl. Acad. Sci. U.S.A. 99 (2002) 15971–15976.
[16] M. Koch, C. Breithaupt, R. Kiefersauer, J. Freigang, R. Huber, A. Messerschmidt, Crystal structure of protoporphyrinogen IX oxidase: a key enzyme in haem and chlorophyll biosynthesis, EMBO J. 23 (2004) 1720–1728.
[17] M.W. Bowler, M.G. Montgomery, A.G.W. Leslie, J.E. Walker, Reproducible improvements in order and diffraction limit of crystals of bovine mitochondrial F_1-ATPase by controlled dehydration, Acta Cryst. D62 (2006) 991–995.
[18] P. Chotiyarnwong, G.B. Stewart-Jones, M. Tarry, W. Dejnirattisai, C. Siebold, M. Koch, D.I. Stuart, K. Harlos, P. Malasit, G. Screaton, J. Mongkolsapaya, E.Y. Jones, Humidity control as a strategy for lattice optimization applied to crystals of HLA-A*1101 complexed with variant peptides from dengue virus, Acta Cryst. F63 (2007) 386–392.
[19] G. Feher, Z. Kam, Nucleation and growth of protein crystals: general principles and assays, Meth. Enzymol. 114 (1985) 77–112.
[20] Z. Otwinowski, W. Minor, Processing of X-ray diffraction data collected in oscillation mode, Meth. Enzymol. 276 (1997) 307–326.
[21] G.N. Murshudov, A.A. Vagin, E.J. Dodson, Refinement of macromolecular structures by the maximum-likelihood method, Acta Cryst. D53 (1997) 240–255.
[22] Collaborative Computational Project, Number 4, The *CCP4* suite: programs for protein crystallography, Acta Cryst. D50 (1994) 760–763.
[23] P. Emsley, K. Cowtan, *Coot*: model-building tools for molecular graphics, Acta Cryst. D60 (2004) 2126–2132.
[24] H.M. Berman, T. Battistuz, T.N. Bhat, W.F. Bluhm, P.E. Bourne, K. Burkhardt, Z. Feng, G.L. Gilliland, S. Iype, S. Jain, P. Fagan, J. Marvin, D. Padilla, V. Ravichandran, B. Schneider, N. Thanki, H. Weissig, D. Westbrook, C. Zardecki, The protein data bank, Acta Cryst. D58 (2002) 899–907.
[25] S. Datta, K. Biswal, M. Vijayan, The effect of stabilizing additives on the structure and hydration of proteins: a study involving tetragonal lysozyme, Acta Cryst. D57 (2001) 1614–1620.
[26] R.A. Laskowski, M.W. MacArthur, D.S. Moss, J.M. Thornton, *PROCHECK*: a program to check the stereochemical quality of protein structures, J. Appl. Cryst. 26 (1993) 283–291.
[27] P.V. Luzzati, Traitement statistique des erreurs dans la determination des structures cristallines, Acta Cryst. 5 (1952) 802–810.
[28] A.A. Vaguine, J. Richelle, S.J. Wodak, *SFCHECK*: a unified set of procedures for evaluating the quality of macromolecular structure-factor data and their agreement with the atomic model, Acta Cryst. D55 (1999) 191–205.
[29] J. Painter, E.A. Merritt, TLSMD web server for the generation of multi-group TLS models, J. Appl. Cryst. 39 (2006) 109–111.
[30] W. Kabsch, A solution for the best rotation to relate two sets of vectors, Acta Cryst. A32 (1976) 922–923.
[31] N.R. Voss, M. Gerstein, 3 V: cavity, channel and cleft volume calculator and extractor, Nucl. Acid. Res. 38 (2010) W555–W562.
[32] M.M. Tirion, Large amplitude elastic motions in proteins from a single-parameter, atomic analysis, Phys. Rev. Lett. 77 (1996) 1905–1908.
[33] F. Tama, F.X. Gadea, O. Marques, Y.-H. Sanejouand, Building-block approach for determining low-frequency normal modes of macromolecules, Protein Struct. Funct. Genet. 41 (2000) 1–7.
[34] M. Gerstein, A. Lesk, C. Chothia, Structural mechanisms for domain movements in proteins, Biochemistry 33 (1994) 6739–6749.
[35] M. Ikeguchi, J. Ueno, M. Sato, A. Kidera, Protein structural change upon ligand binding: linear response theory, Phys. Rev. Lett. 94 (2005) 1–4 078102.
[36] S. Hayward, N. Go, Investigating protein dynamics in collective coordinate space, Annu. Rev. Phys. Chem. 46 (1995) 223–250.
[37] F. Tama, Y.-H. Sanejouand, Conformational change of proteins arising from normal mode calculations, Protein Eng. 14 (2001) 1–6.
[38] I. Bahar, T.R. Lezon, L.-W. Yang, E. Eyal, Global dynamics of proteins: bridging between structure and function, Annu. Rev. Biophys. 9 (2010) 23–42.
[39] M. Nakasako, F. Tsuchiya, Y. Arata, Roles of hydration water molecules in molecular packing of the killer toxin from *Pichia farinose* in its crystalline state investigated by cryogenic X-ray crystallography, Biophys. Chem. 95 (2002) 211–225.
[40] D. Matsuoka, M. Nakasako, Probability distributions of hydration water molecules around polar protein atoms obtained by a database analysis, J. Phys. Chem. B113 (2009) 11274–11292.
[41] M. Nakasako, M. Odaka, M. Yohda, N. Dohmae, K. Takio, N. Kamiya, I. Endo, Tertiary and quaternary structures of photoreactive Fe-type nitrile hydratase from *Rhodococcus* sp. N-771: roles of hydration water molecules in stabilizing the structures and the structural origin of the substrate specificity of the enzyme, Biochemistry 38 (1999) 9887–9898.
[42] M. Nakasako, T. Fujisawa, S. Adachi, T. Kudo, S. Higuchi, Large-scale domain movements and hydration structure changes in the active-site cleft of unligated glutamate dehydrogenase from *Thermococcus profundus* studied by cryogenic X-ray crystal structure analysis and small-angle X-ray scattering, Biochemistry 40 (2001) 3069–3079.
[43] M. Nakasako, Large-scale networks of hydration water molecules around bovine β-trypsin revealed by cryogenic X-ray crystal structure analysis, J. Mol. Biol. 289 (1999) 547–564.
[44] V.N. Morozov, G.S. Kachalova, V.U. Evtodienko, N.F. Lanina, T.Ya. Morozova, Permeability of lysozyme tetragonal crystals to water, Eur. Biophys. J. 24 (1995) 93–98.
[45] A. Zamiri, S. De, Modeling the mechanical response of tetragonal lysozyme crystals, Langmuir 26 (2010) 4251–4257.
[46] S. Speziale, F. Jiang, C.L. Caylor, S. Kriminski, C.-S. Zha, R.E. Thorne, T.S. Duffy, Sound velocity and elasticity of tetragonal lysozyme crystals by Brillouin spectroscopy, Biophys. J. 85 (2003) 3202–3213.
[47] P.S. Kaushal, R. Sankaranarayanan, M. Vijayan, Water-mediated variability in the structure of relaxed-state haemoglobin, Acta Cryst. F64 (2008) 463–469.
[48] M. Ueda, Rate of evaporation of water by forced convection, Appl. Phys. (in Japanese) 29 (1969) 443–451.
[49] D.W. Grover, J.M. Nicol, The vapor pressure of glycerine solutions at 20 °C, J. Soc. Chem. Ind. 59 (1940) 175–177.
[50] B.W. Matthews, Solvent content of protein crystals, J. Mol. Biol. 33 (1968) 491–497.
[51] A.T. Brünger, Free *R* value: a novel statistical quantity for assessing the accuracy of crystal structures, Nature 355 (1992) 472–474.
[52] W.L. DeLano, PyMOL, http://www.pymol.org (2002).
[53] L. Potterton, S. McNicholas, E. Krissinel, J. Gruber, K. Cowtan, P. Emsley, G.N. Murshudov, S. Cohen, A. Perrakis, M. Noble, Developments in the *CCP*4 molecular-graphics project, Acta Cryst. D60 (2004) 2288–2294.